


Fibroblast Growth Factor 21 Protects Against Cerebral Ischemia/Reperfusion Injury by Inhibiting Oxidative Stress and Ferroptosis

Junjie Li*, Haiyan Jiang*, Wenya Bai, Yuan Yang, Guilin Zhou, Wendong Chen , Jianlin Shao

Department of Anesthesiology, the First Affiliated Hospital of Kunming Medical University, Kunming City, Yunnan Province, People's Republic of China

*These authors contributed equally to this work

Correspondence: Jianlin Shao; Wendong Chen, Department of Anesthesiology, the First Affiliated Hospital of Kunming Medical University, 295 Xichang Road, Wuhua, Kunming, Yunnan, 650000, People's Republic of China, Tel +86-0871-6532488-2755, Email cmushaojlmz@163.com; chenwendong@ydy.cn

Purpose: Cerebral ischemia/reperfusion injury (CIRI) severely impacts patient outcomes and quality of life, with limited treatment options. Although fibroblast growth factor21 (FGF21) is known for its metabolic and anti-inflammatory effects, its role and mechanisms in CIRI are not well explored.

Methods: After developing an MCAO/R injury model, mice received intraperitoneal injections of FGF21 (1.5 mg/kg) 15 min pre-reperfusion, as well as 8 and 16 h post-reperfusion. The TTC, TUNEL, H&E, and Nissl stainings were used 24 h post-reperfusion to determine the infarct volume, apoptotic cells, brain pathological damage, and nerve cell survival, respectively. ELISA and Western blotting were employed to detect oxidative stress (OxS) products and ferroptosis-related markers. RNA-seq of the ischemic penumbra tissues was conducted, followed by bioinformatics analysis to screen and identify differentially expressed genes (DEGs). Then, we used qPCR to validate relevant molecule mRNA expression while using immunofluorescence staining to assess CYBB protein localization and expression.

Results: The FGF21 reduced the infarct volume in MCAO/R-injured mice, diminished apoptotic cell numbers, and alleviated pathological damage to ischemic brain tissue. Furthermore, FGF21 inhibited OxS and ferroptosis post-CIRI. RNA-seq revealed a significant differential expression of numerous genes, extensively involving diverse biological processes post- ischemia/reperfusion injury (IRI). Bioinformatics analysis and validation results indicated that CYBB was the most significantly differentially expressed ferroptosis-related molecule, and it may be a novel key regulatory molecule mediating anti-IRI of FGF21.

Conclusion: FGF21 protects CIRI by inhibiting OxS and ferroptosis. The CYBB, a new key regulator, may mediate its anti-ferroptotic effects, offering new insights into CIRI therapies.

Keywords: FGF21, cerebral ischemia/reperfusion injury, oxidative stress, ferroptosis, CYBB

Introduction

On a global scale, stroke has emerged as the second major driver of mortality and the third of disability. Over the past thirty years, stroke annual incidence and mortality rates have surged worldwide. Notably, ischemic stroke accounts for the highest proportion, constituting 62.4% of all stroke events in 2019, imposing a significant burden on patients and society.¹ While timely reperfusion therapy can restore blood flow following cerebral ischemia, this intervention often comes with ischemia/reperfusion (I/R) injury, which significantly diminishes treatment efficacy and elevates patient mortality rates.² Recently, numerous studies have explored various therapeutic strategies for cerebral I/R injury (CIRI), encompassing pharmacological approaches such as utilizing glutamate antagonists, nicotinamide, and salvianolic acid B (Sal B) to restore energy metabolism and inhibit apoptosis; mitochondrial-based treatments like stem cell-derived mitochondrial transplantation; and traditional Chinese medicine (TCM) interventions including acupuncture and monotherapy with herbal compounds. However, given the multifactorial nature of CIRI and the uncertain toxic and side effects

of some medications, monotherapy may be insufficient. Additionally, the clinical application of TCM in treating CIRI is limited due to the lack of evidence-based medical support.^{3,4} Therefore, the continuous exploration and development of effective therapeutic strategies to alleviate CIRI is clinically crucial.

Among the diverse mechanisms implicated in CIRI, ferroptosis, an iron-dependent, non-apoptotic cell death, has garnered substantial attention from researchers recently.⁵ Extensive research evidence has underscored the significance of ferroptosis in CIRI pathogenesis. Cerebral I/R (CIR) significantly elevated free iron and reactive oxygen species (ROS) levels within the brain tissue, which is intimately linked to ferroptosis initiation and progression.^{6,7} The evolution of CIRI enhances susceptibility to oxidative stress (OxS) and disrupts ATP production, a crucial molecule for maintaining cellular metabolic activity and the functionality of the Xc-antioxidant system. This injury is associated with iron accumulation, lipid oxidative damage, and decreased levels of antioxidants GSH and GPX4. The lethal imbalance resulting from GSH depletion and GPX4 inactivation triggers ferroptosis in neurons and other brain cells. Additionally, the abundance of Fe²⁺ ions in the post-stroke brain may further catalyze lipid ROS formation via the Fenton reaction, exacerbating OxS and ultimately leading to iron-induced cell death and neuronal damage.^{8,9} Furthermore, studies have revealed that the frequently utilized OxS stimulant tert-butyl hydroperoxide can trigger neuronal cell death, whereas ferroptosis inhibitor serves as a blocker of this death pathway, suggesting an interplay between initial oxidative damage and ferroptosis.¹⁰ Therefore, strategies aimed at blocking OxS and ferroptosis hold promise for ameliorating CIRI.

The FGF21, primarily secreted by the liver as an endocrine factor, exerts beneficial effects through multiple biological actions, including enhancing glucose uptake, regulating energy metabolism, exhibiting anti-inflammatory properties, and maintaining mitochondrial stability.^{11–15} Furthermore, FGF21 possesses robust capabilities to penetrate the blood-brain barrier (BBB), readily diffusing into the brain to contribute to metabolic regulation, neuroprotection, and cognitive functions.^{16,17} Consequently, in the context of CIRI, FGF21 may hold potential therapeutic advantages. Presently, numerous studies have delved into the FGF21 neuroprotective effects. By modulating metabolism and exerting anti-inflammatory actions, FGF21 has been manifested to mitigate neurocognitive malfunction in high-fat diet-fed mice.¹⁸ It mitigates neuroinflammation and OxS by regulating the NF- κ B and AMPK α /AKT pathways, thereby reducing neurodegeneration and enhancing the protection of neuronal mitochondria in aging mice.¹⁹ Furthermore, rhFGF21 significantly ameliorates neurofunctional behavioral deficits and reduces the degree of cerebral edema in mouse models of traumatic brain injury, preserving BBB integrity and decreasing cerebral tissue loss and neuronal apoptosis.²⁰ Notably, FGF21 has been shown to inhibit iron overload by regulating iron metabolism-related protein expression, thereby protecting cells from damage induced by iron poisoning.^{21,22} These conclusions construct a theoretical foundation for applying FGF21 in CIRI treatment.

Nonetheless, FGF21's involvement and mechanism in CIRI is still vague. Accordingly, we aimed to reveal the potential of FGF21 to ameliorate CIRI and inhibit ferroptosis in neuronal cells following such injury. Herein, FGF21 was administered to a murine model of CIR to assess its effects on the injury and identify key molecules involved through transcriptomic sequencing and subsequent validation. Moreover, we anticipate that this study will offer novel insights and an experimental foundation for the application of FGF21 in addressing CIRI, thereby contributing to developing innovative therapeutic strategies for ischemic brain injury.

Material and Methods

Animals and Ethical Statement

Herein, C57BL/6 adult male mice (SPF, 20 \pm 2 g, 6–8 weeks; Biotechnology Co., Ltd., Beijing, China) were adaptively fed at 21–25 °C and a 12-h light-dark cycle, with free water and food access for 1 week before surgery, making every effort to minimize animal suffering besides keeping mice numbers to a minimum. The study adhered to the NIH guidelines for the Care and Use of Laboratory Animals and was authorized by the Animal Ethics Committee of Kunming Medical University (approval no.: Kmmu20240567).

Establishment of Middle Cerebral Artery Occlusion/ Reperfusion (MCAO/R) Model

The MCAO/R mice model was constructed as outlined earlier.²³ Briefly, following anesthesia with 2% isoflurane at a 0.4 L/min flow rate, we made an incision through the mice's neck skin, seeking the exposure of the right common carotid

artery (CCA) and internal/external carotid artery [(ICA)/(ECA)]. The CCA was ligated at the proximal end, and the ECA was tied and severed at the distal end. A nylon wire (L1800, Jialing Biotechnology, Guangzhou) was introduced into the ECA notch and advanced in the ICA direction until resistance was encountered. The nylon wires were withdrawn following 1 h of induced ischemia. Throughout the procedure, the mice were placed on a thermal blanket to sustain a normal body temperature of 36.5 ± 0.5 °C. Following a previous study,²⁴ mice were evaluated on a Zea-Longa scale after waking, and those scoring 0 or 4 were excluded. Then, 24 h post-reperfusion, the mice were exposed to deep anesthesia prior to being euthanized. Blood and brain tissue from the mice were harvested for subsequent experiments.

Experimental Grouping and FGF21 Management Protocol

Mice were assigned at random into three groups ($n = 5/\text{group}$), with the sample size determined using the resource equation approach based on previously established methods for calculating sample sizes in animal experiments.²⁵ Randomization was performed using a digital table method. To maintain double-blinding, two independent teams were involved: one team was responsible for assigning group numbers and conducting the modeling on the animals, while the other team carried out the experimental testing. The group assignments and treatments were as follows: Sham (an incision was made in the neck only, the CCA was exposed, and an equal NS volume was administered), MCAO/R (the MCAO/R model was treated with the same NS volume), and MCAO/R+FGF21 groups (the MCAO/R model was treated with FGF21). The methodology and FGF21 dosages used were based on prior studies of FGF21 in treating BBB injury and ventilator-induced lung injury.^{20,26} Briefly, recombinant mouse FGF21 (1.5 mg/kg, P6101, Beyotime, Shanghai, China) was dissolved in PBS and injected intraperitoneally 15 min pre-reperfusion, 8 and 16 h post-reperfusion.

2,3,5-Triphenyltetrazolium Chloride (TTC) Staining

Initially, the whole brain was frozen at -80 °C for 30 min, thawed for nearly 2 min at room temperature (RT), sectioned into five equal slices placed in a flask with 20 mL of 2% TTC solution (G3005, Solarbio, Beijing), and stained in a light-protected box for 20 min at 37 °C. Following the staining procedure, the staining solution was discarded, followed by gradually adding 4% paraformaldehyde (PFA) solution to the flask. The reaction was halted and temporarily kept in the dark, with color images being captured after 24 h. The infarcted areas on each slice were assessed and quantified by Image J software (version 1.43), with the proportion of cerebral infarction volume calculated according to previously described methods.²⁷

Hematoxylin-Eosin (H&E) Staining

The paraffin-embedded tissue blocks were sectioned into 4–6 μm slices, placed on slides, dewaxed in xylene, and rehydrated with alcohol. The sections were subjected to hematoxylin staining (G1004-100ML, Servicebio, Wuhan) for 2 min to color the chromatin and ribosomes purplish blue, then rinsed with water to remove excess dye. The slices were immersed in 1% hydrochloric ethanol for 15s to remove excess stain, then treated with ammonia water for 15s to restore the blue nucleus color. After washing with running water for 5 min, the sections were subjected to 0.5% eosin staining (G1108, Solarbio, Beijing) for 1–3 min, re-rinsed again, dehydrated, sealed with neutral resin, dried, and observed by a microscope.

Nissl (Thionin) Staining

Following a 48-h fixation in 4% PFA, we coronally sectioned the paraffin-embedded brain tissues. Subsequently, the brain sections were dewaxed and incubated with Nissl Stain Solution (Thionin, G1438, SolarBio, Beijing) at 56 °C for 1 h. This was followed by a 2-min treatment with Nissl differentiation solution (SolarBio), immersing in xylene for 20 min, rinsing with distilled water, air drying, and photographing under a microscope.

TUNEL Staining

Paraffin sections were dewaxed, hydrated, fixed in 4% PFA for 10 min, and rinsed with PBS. Each sample was covered with 100 μL of 20 $\mu\text{g}/\text{mL}$ Proteinase K solution, followed by incubation at 37 °C for 20 min and PBS wash. The TUNEL reaction solution (C1098, Beyotime, Shanghai) was prepared per instructions, added dropwise to the sample, and

incubated in darkness, humid chamber at 37 °C for 1 h. The sample was then washed with PBS to eliminate the unbound TUNEL solution. The DAB was added for 1–2 min until apoptotic cells turned brown, then rinsed with PBS to stop the staining. The slides were subjected to hematoxylin staining for 5 min, rinsed with distilled water, differentiated in alcohol hydrochloric acid for 10–15s, and placed in tap water for at least 15 min. Following dehydration and transparency, the slides were sealed using neutral gum and observed by a microscope. Five random 400 X visual fields were selected to count TUNEL positive and total cells, and the apoptotic cell rate per field was calculated.

Elisa Analysis

Following the protocols of commercial ELISA kits, Oxs products in serum and brain tissue, along with Fe^{2+} in brain tissue, were determined: MDA (CB10205-Mu), ROS (CB10366-Mu, both from COIBO BIO), MPO (MM-0338M2, Meimian Industrial, Jiangsu), SOD (MM-0389M2, Meimian), Fe^{2+} (JLCS102569), GSSG (JLCS102569), and GSH (JLCS1500, the three from Jingkang Bioengineering). The optical density (OD) of each well was measured at a wavelength of 450 nm, and the concentration of each molecule was subsequently determined.

Western Blotting

Proteins from ischemic penumbra brain tissue (50 mg) were extracted by RIPA lysates (Servicebio, Wuhan, China) with protease inhibitors (Servicebio). The total protein levels were evaluated with a BCA kit (Beyotime, Shanghai, China). The proteins were separated by 10% SDS-PAGE (Beyotime). For SDS-PAGE, start with 80 V for 30 minutes. Increase to 120 V when samples reach the resolving gel. Continue until the dye reaches the gel's bottom, about 90 minutes, then remove the gel and transferred to PVDF membranes (Millipore, USA) blocked with 5% bovine serum albumin (BSA; Solarbio, Beijing, China) for 1 h at RT. After washing with TBST, primary antibodies ACSL4 (1:1000, rabbit, DF12141, Affinity, AUS), GPX4 (1:1000, rabbit, ET1706-45, HUABIO, Hangzhou, China), CYBB (1:1000, rabbit, bs-3889R, Bioss, Beijing, China) and β -Actin (1:2500, mouse, 66009-1-Ig, Proteintech, USA) were introduced and incubated at 4 °C for a whole night. Following a 2-h incubation with an HRP-labeled secondary antibody (1:2000, CST 7074 or 7076, CST, USA), the membranes were rewashed. Protein bands were visualized with ECL (Millipore, USA) in a gel imaging system to obtain the original images with three different exposure times (7, 14, and 21s). Image J (Ver.1.3) was utilized to measure the gray value, using the ratio of target proteins to β -Actin gray values to determine their relative expression levels.

qPCR

Total RNA extraction from ischemic penumbra brain tissue was performed with TRIzol reagent (Ambion, USA), quantified, and then stored at –80 °C. Following the protocols, Slc7a11, Slc39a14, Stat3, and Cybb were reversely transcribed with the SureScript First-Strand cDNA Synthesis Kit (Servicebio, China) through a conventional PCR machine (Thermo Fisher Scientific, USA) at 25 °C for 5 min, 42 °C for 15–30 min, 85 °C for 5s; and then held at 4 °C. The qRT-PCR reactions were conducted on a CFX96 instrument (Bio-Rad, USA) equipped with 2x Universal Blue SYBR Green qPCR Master Mix (Servicebio, China) to detect relative mRNA levels. The amplification reaction conditions included the following: initial denaturation at 95 °C for 1 min, 40 cycles of denaturation at 95 °C for 20s, annealing at 55 °C for 20s, and extension at 72 °C for 30s. Fluorescence signals were retrieved after 40 cycles to generate amplification and melting curves, and Ct values were recorded. GAPDH served as the internal reference gene, thereby calculating the relative fold changes of target genes by the $2^{-\Delta\Delta\text{Ct}}$ method. All gene primers were synthesized by Qingdao BioTech Co., Ltd. in Kunming, China: Slc7a11: F- GCC CTGTCCTATGCAGAATTAG, R- AGTAGCTCCAGGGCGTATTA; Slc39a14: F- GACTTCGTCATCCTGCTCAAT, R- CCAAAGGCCAGACCCAAATA; Stat3: F- ACCAACGACCTGCAGCAATA, R- TCCATGTCAAACGTGAGCGA; Cybb: F- TCAGTGAGCTTCCCTGTGTC, R- GCATTTCGCTTCGGTGATGT.

Immunofluorescence Staining

The paraffin-embedded tissue sections were placed in a 64 °C incubator for 1 h and immersed in xylene and alcohol solutions for dewaxing and hydration, respectively. Subsequently, citrate buffer solution was used to complete antigen retrieval, followed by incubation in a prepared permeabilization solution at RT for 20 min to inactivate endogenous

peroxidase activity. Following PBS washing, the slides were blocked with 5% BSA at 37 °C for 30 min. The primary antibodies were diluted with 2% BSA at a 1:100 ratio using CYBB (1:100, rabbit, bs-38R, Bioss, Beijing, China) and NeuN (1:100, rabbit, bs-10394R, Bioss). The diluted primary antibodies were dropped onto the slides and incubated in a 4°C refrigerator for a whole night. Then, the slides were rewarmed in a 37 °C incubator for 30 min before rinsing with PBS. Goat anti-rabbit IgG H&L (ab150078, Abcam) secondary antibody was introduced and incubated at 37 °C for 30 min, followed by PBS rinsing. Then, the cells were stained with DAPI solution for 5 min at RT in darkness, followed by PBS rinsing. Eventually, the slides were mounted with an anti-fade mounting medium, observed, and images were captured under a microscope.

RNA-Seq and Differentially Expressed Genes (DEGs) Analysis

Per the protocols, total RNA was isolated and purified with TRIzol (ThermoFisher, 15596018), thereby determining its quantity and purity via NanoDrop ND-1000 (NanoDrop, Wilmington, DE, USA) while assessing its integrity using Bioanalyzer 2100 (Agilent, CA, USA), ensuring a concentration > 50ng/μL, RIN > 7.0, and total RNA > 1μg. The mRNA with PolyA (polyadenylate) tails was captured with oligo(dT) magnetic beads (Dynabeads Oligo (dT), cat.25–61005, Thermo Fisher, USA) via two purification rounds. The mRNA was fragmented at 94 °C for 5–7 min using the NEBNextR RNA Fragmentation Module (E6150S, USA), followed by synthesizing the cDNA by Invitrogen SuperScript™ II Reverse Transcriptase (1896649, CA, USA). The E. coli DNA polymerase I (NEB, m0209, USA) and RNase H (NEB, m0297, USA) were used to create double-stranded DNA from the cDNA. The dUTP Solution (R0133, Thermo Fisher, CA, USA) was introduced to these double strands to produce A-overhangs, allowing for a T-base terminal connection. Finally, we screened and purified the fragment size utilizing magnetic beads. The two chains were digested by UDG enzyme (NEB, m0280, MA, US) and subjected to PCR: 95 °C for 3 min, 8 cycles of 98 °C for 15s, 60 °C for 15s, and 72 °C for 30s, followed by a final extension at 72 °C for 5 min to form a 300 ± 50 bp library (chain specific library). Sequencing was carried out via Illumina NovaSeq™ 6000 in PE150 mode.

Differential gene expression analysis between two groups (and by edgeR between two samples) was conducted using DESeq2. OmicStudio tools (<https://www.omicstudio.cn/tool>) were utilized to plot normalized FPKM values in an advanced volcano plot on the basis of log₂(fold change) and -log₁₀(q value), with thresholds of |log₂(FC)| ≥ 1.0 and q < 0.05. The hierarchical clustering of DEGs produced an overall clustering heat map for the samples. The GO enrichment analysis was conducted on DEGs, and the first 50 GO terms with the smallest q-value were selected to draw a histogram. The DEGs were analyzed by the KEGG Orthology-Based Annotation System (KOBAS) for KEGG enrichment, and then the bubble map was drawn. Next, Reactome enrichment analysis of differential genes was performed using the Reactome database (<https://reactome.org>, v76) to study the enrichment of genes in biological pathways. Finally, we retrieved 484 ferroptosis-correlated genes by accessing the FerrDb database (<http://www.zhounan.org/ferrdb/>). Using a Venn diagram, significantly different genes were identified for further analysis.

Statistical Analysis

Statistical analysis and data visualization were performed through GraphPad Prism (Version 6.0), reporting data as mean ± standard deviation. Comparative analyses between the two groups were performed utilizing a two-tailed *t*-test, with *P* < 0.05 indicating significance.

Results

FGF21 Significantly Attenuated Cerebral Infarction Extent and Reduced Apoptotic Cell Numbers in I/R Mice

The TTC staining results showcased that the MCAO/R group displayed a significantly increased volume proportion of cerebral infarction relative to the Sham group (33.64 ± 0.74% vs 0.00 ± 0.00%). In comparison to the MCAO/R group, FGF21 significantly lowered the volume proportion of cerebral infarction (17.25 ± 0.57% vs 33.64 ± 0.74%, [Figure 1A](#)). The results of TUNEL staining manifested that the MCAO/R group displayed significantly increased apoptotic cell

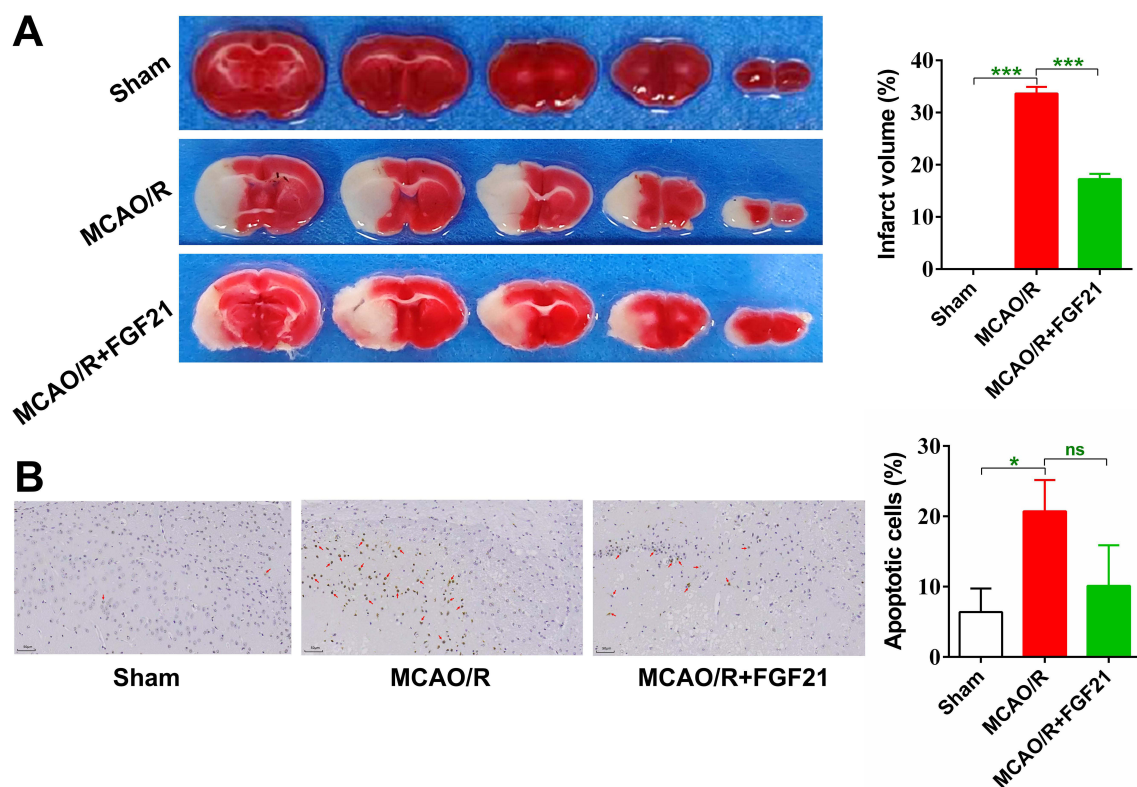


Figure 1 FGF21 reduces the cerebral infarction volume and decreases the number of apoptotic cells in mice with IRI. **(A)** TTC staining: Cerebral infarction. **(B)** TUNEL staining: Cellular apoptosis. Data represent Mean \pm SD. (n=5). * $P < 0.05$, *** $P < 0.001$, ns, no significance. The red arrows: TUNEL positive cells (apoptotic cells).

number, unlike the Sham group (Apoptotic cell ratio: $20.72 \pm 2.56\%$ vs $6.378 \pm 1.95\%$). However, FGF21 reduced apoptotic cell numbers in contrast to the MCAO/R group (Apoptotic cell ratio: $10.11 \pm 3.34\%$ vs $20.72 \pm 2.56\%$, Figure 1B).

FGF21 Alleviated the Pathological Damage to Brain Tissue and Improved the Survival of Nerve Cells in I/R Mice

Both H&E and Nissl stainings were utilized to assess pathological lesions and the viability of neuronal cells in brain tissue, respectively. The findings from H&E staining indicated that neuronal cells in the Sham group exhibited orderly arrangement, intact structure, and a round or oval morphology with uniform staining. The cytoplasm appeared pink, while the nucleus was stained a vivid purple by hematoxylin, revealing a distinct nuclear membrane and nucleolus. Following IRI, nerve cell number was significantly reduced, accompanied by disorganized cellular arrangement, morphological alterations, and manifestations of cellular swelling, atrophy, and deformation. Conversely, treatment with FGF21 significantly ameliorated cell morphology and arrangement, significantly mitigating cellular damage (Figure 2A). The results of Nissl staining indicated that the nerve cells in the Sham group exhibited an intact structure and orderly arrangement, with a significant presence of blue-purple Nissl bodies. Following IRI, the viable neuron number was significantly reduced, characterized by the disappearance of numerous lysed Nissl bodies and the presence of heavily stained cell fragments. However, treatment with FGF21 significantly ameliorated these conditions, evidenced by an increased number of surviving cells and Nissl bodies (Figure 2B).

FGF21 Attenuated OxS in Mice With IRI

The OxS product concentration in the mice serum was measured using an ELISA kit. Unlike the Sham group, the serum concentrations of the pro-OxS markers MDA, MPO, and ROS significantly escalated in the MCAO/R group (Figure 3A–C). Nevertheless, FGF21 treatment significantly reduced these concentrations relative to the MCAO/R group (Figure 3A–C).

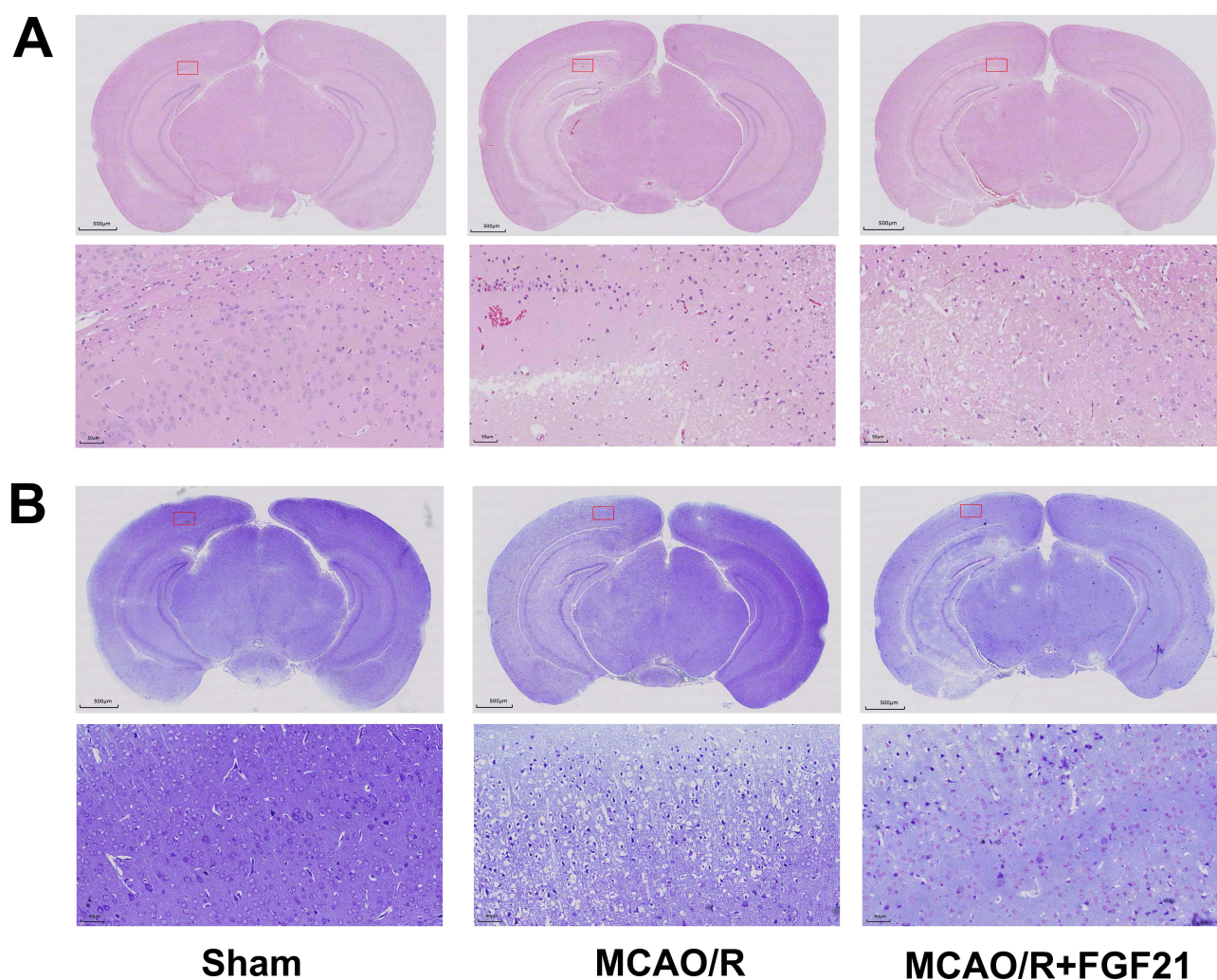


Figure 2 FGF21 attenuates pathological damage to the brain tissue and neuronal injury in CIR mice. **(A)** H&E staining: Pathological damage to the brain tissue. **(B)** Nissl staining: Neuronal survival. Scale bar: 500 and 50 μ m (low- and high-magnification images). The red box: Acquisition area for the high-magnification image.

Conversely, the antioxidant SOD concentration was significantly reduced in the MCAO/R group in contrast to the Sham group, but it increased post-FGF21 treatment (Figure 3D).

FGF21 Prevented Ferroptosis in Nerve Cells Following IRI in Mice

The Fe^{2+} concentration and ferroptosis-related marker expression in ischemic penumbra brain tissues of mice were ascertained by ELISA and Western blot, respectively. In comparison to the Sham group, the concentrations of ROS (Figure 4A), Fe^{2+} (Figure 4B), and GSSG (Figure 4C) in the brain tissue of the MCAO/R group were significantly heightened, and ACSL4 protein was significantly overexpressed (Figure 4E and F). The GSH concentration was significantly diminished (Figure 4D), and GPX4 protein was significantly suppressed (Figure 4E and G). Nonetheless, compared with the MCAO/R group, the concentrations of ROS (Figure 4A), Fe^{2+} (Figure 4B), and GSSG (Figure 4C) in brain tissue after FGF21 treatment were significantly diminished, and ACSL4 protein was significantly repressed (Figures 4E and F). The concentration of GSH was significantly elevated (Figure 4D), and GPX4 protein was significantly overexpressed (Figure 4E and G). Altogether, FGF21 can inhibit nerve cell ferroptosis after I/R.

RNA-Sequencing (RNA-Seq) and Screening of DEGs in Mouse Penumbra Brain Tissue

To explore the molecular mechanism of FGF21's role in CIRI, RNA-Seq and bioinformatics analysis were conducted on ischemic penumbra brain tissues from three groups of mice to identify gene expression differences. In contrast to the Sham

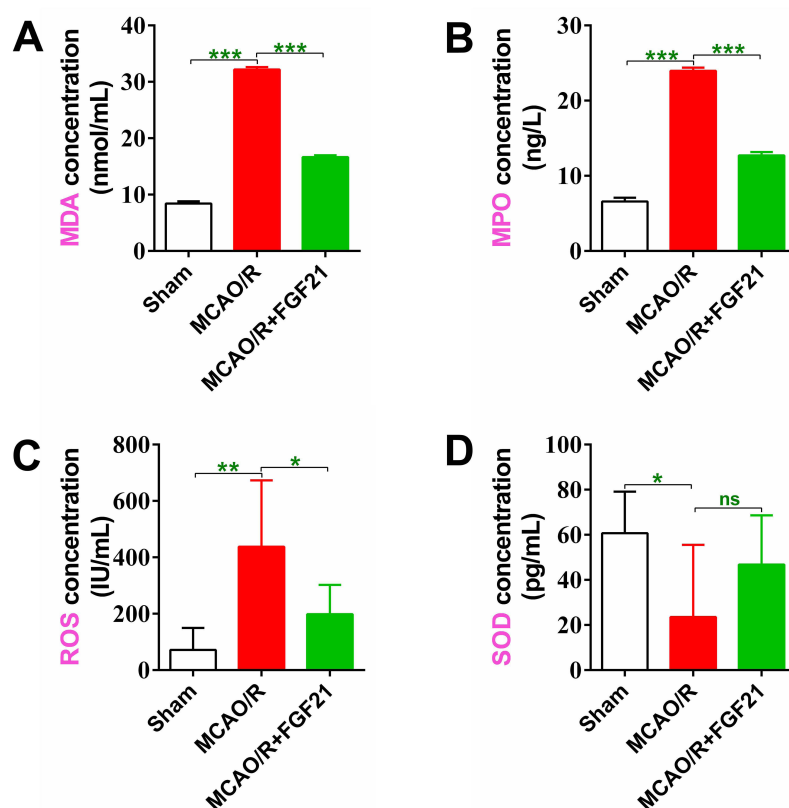


Figure 3 Inhibitory effect of FGF21 on oxidative stress (OxS) in mice post-IRI. ELISA: Levels of OxS products in the serum: (A) MDA, (B) MPO, (C) ROS, and (D) SOD. Data represent Mean \pm SD. (n=5). * $P < 0.05$, ** $P < 0.01$, *** $P < 0.001$, ns, no significance.

group, the MCAO/R group displayed 3023 significant DEGs: 2266 were overexpressed, and 757 were suppressed (Figure 5A). The MCAO/R+FGF21 group had 2480 significant DEGs compared with the MCAO/R group: 601 were up-regulated, and 1879 were down-regulated (Figure 5B). Further Hierarchical Cluster method was used to cluster differential genes (Figure 5C and D), obtaining the clustering results of DEGs (the 50 genes with the lowest q value).

Comprehensive Bioinformatic Analysis Encompassing GO, KEGG, and Reactome Pathway Enrichment of DEGs

The GO enrichment analysis results manifested that after IRI, unlike the Sham group: (1) In terms of biological processes (BP), the DEGs exhibited a main enrichment in signal transduction, regulation of transcription, and DNA-templated and positive regulation of transcription by RNA polymerase II, among others; (2) In terms of cell components (CC), DEGs were mainly enriched in the membrane, cytoplasm, integral component of membrane and nucleus, among others; (3) In terms of molecular function (MF), DEGs exhibited a main enrichment in protein binding, metal ion binding, identical protein binding, and DNA binding, among others (Figure 6A). Compared with the MCAO/R group, after FGF21 treatment, (1) In terms of BP, DEGs exhibited a main enrichment in signal transduction, positive regulation of transcription by RNA polymerase II, regulation of transcription, and DNA-templated and multicellular organism development, among others; (2) In terms of CC, DEGs exhibited a main enrichment in membrane, integral component of membrane, and cytoplasm and plasma membrane, among others; (3) In terms of MF, DEGs exhibited a main enrichment in protein binding, metal ion binding, and identical protein binding and transferase activity, among others (Figure 6D).

The findings of KEGG pathway enrichment analysis elucidated that (the top 30 most significant pathways) compared with the Sham group, after IRI, the DEGs were mainly enriched in complement and coagulation cascades, hypertrophic cardiomyopathy, dilated cardiomyopathy, TGF- β signaling, NF- κ B signaling, cAMP signaling, and Ferroptosis and Toll-like receptor signaling, among others (Figure 6B). Compared with the MCAO/R group, after FGF21 treatment, DEGs

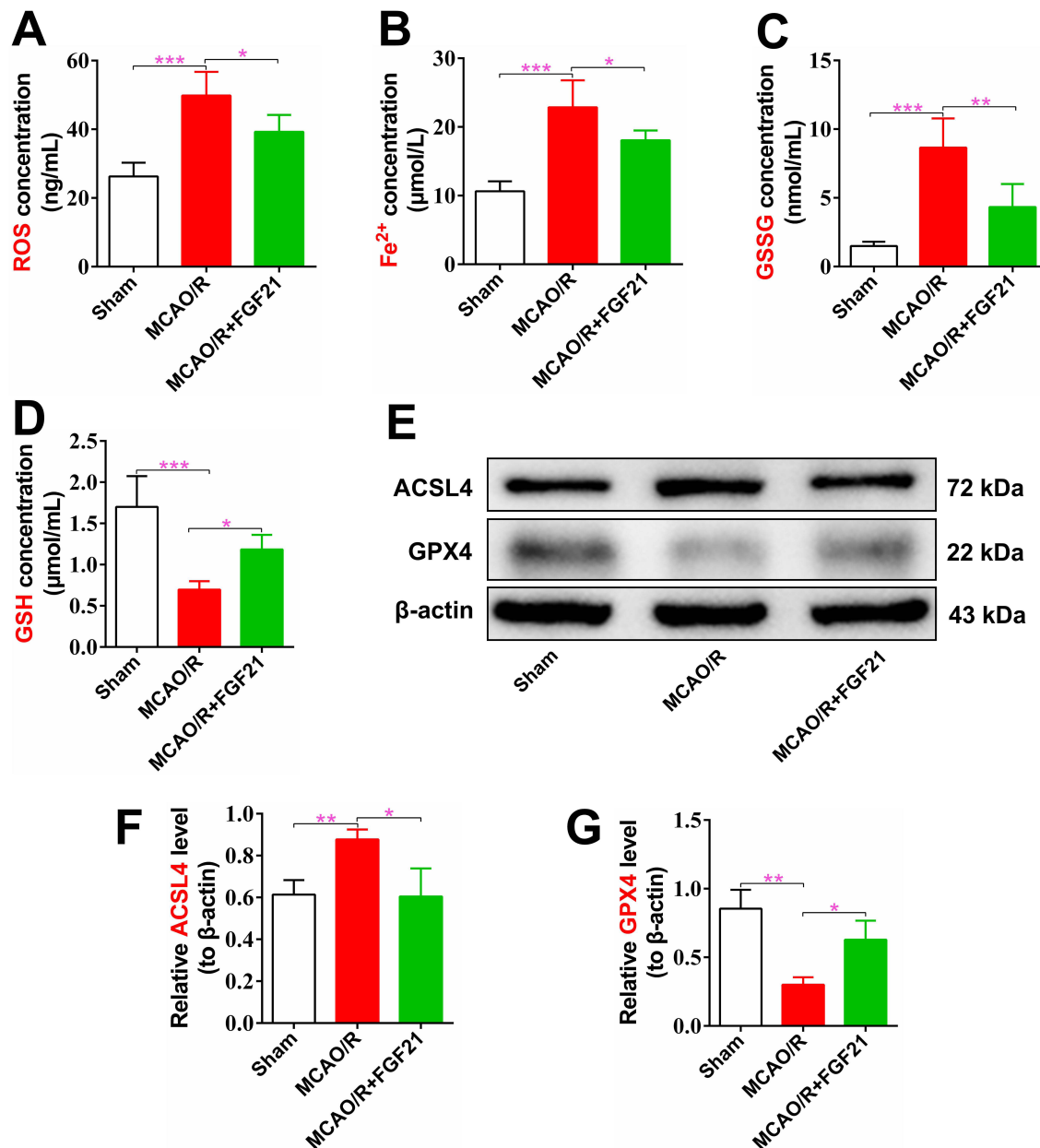


Figure 4 FGF21 inhibits ferroptosis in mouse brain tissue post-IRI. ELISA: (A) Concentration of ROS, (B) Fe²⁺, (C) GSSG, and (D) GSH. Western blotting: (E) bands of ferroptosis-related proteins, (F) expression levels of ferroptosis-promoting protein ACSL4 and (G) ferroptosis-inhibiting protein GPX4. Data represent Mean ± SD; (n = 5). **P* < 0.05, ***P* < 0.01, ****P* < 0.001.

were mainly enriched in neuroactive ligand-receptor interaction, signaling pathways regulating pluripotency of stem cells, cAMP pathway, complement and coagulation cascades, PPAR pathway, cGMP-PKG signaling, and Ferroptosis and TGF-β signaling, among others (Figure 6E).

Furthermore, we analyzed DEGs with Reactome enrichment analysis to reveal the enrichment degree of the selected differential gene set in specific biochemical reactions or signaling pathways. In comparison to the Sham group, after IRI, multiple up-regulated genes were involved in signal transduction, immune system, metabolism, innate immune system, metabolism of proteins, and post-translational protein modification, among others; several down-regulated genes contributed to signal transduction, immune system, metabolism, signaling by GPCR, GPCR downstream signaling and metabolism of proteins, among others (Figure 6C). On the other hand, compared with the MCAO/R group, after FGF21 treatment, up-regulated genes were mainly enriched in signal transduction, metabolism, signaling by GPCR, GPCR downstream signaling and metabolism of proteins, metabolism of proteins and GPCR ligand binding, among others; The

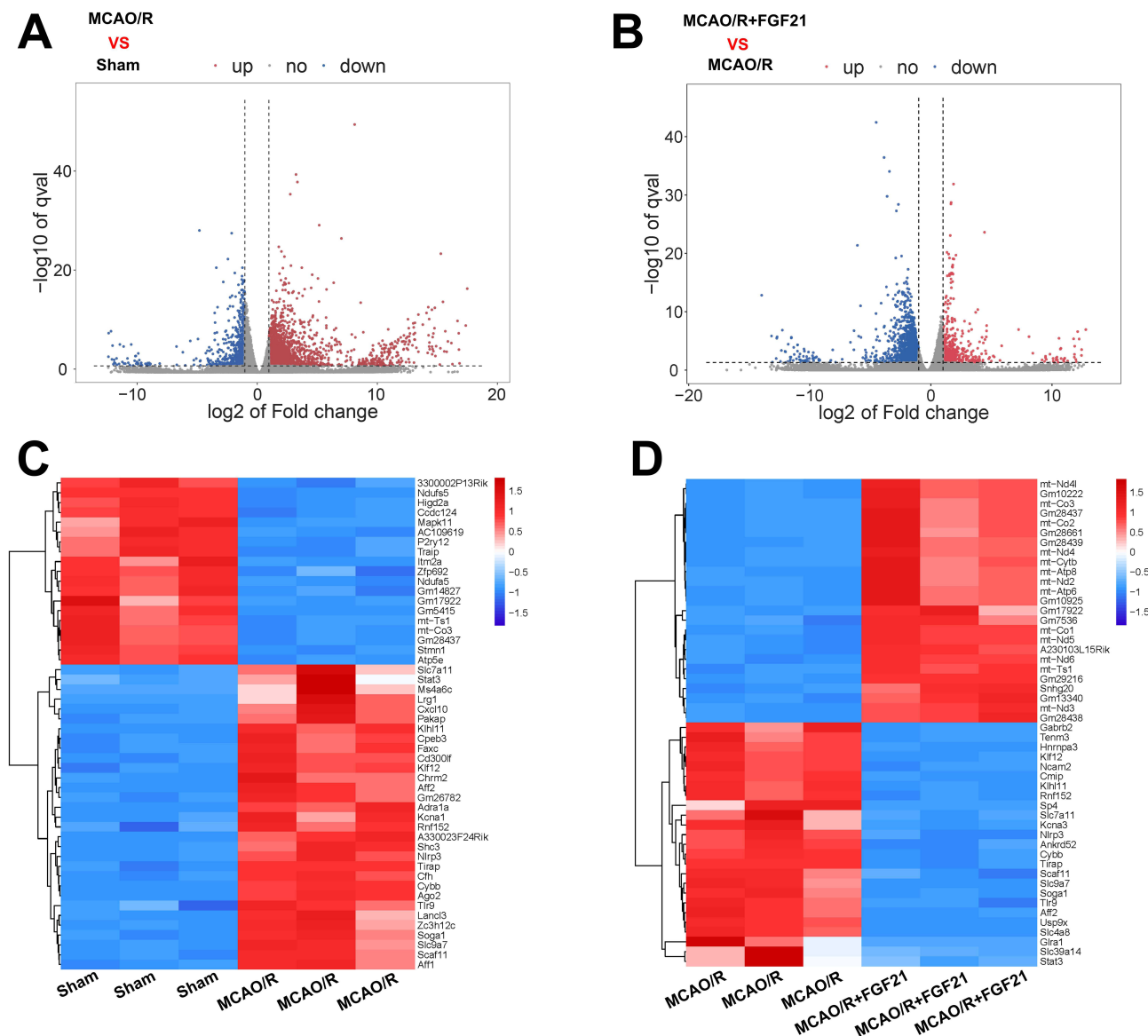


Figure 5 RNA sequencing of ischemic penumbra tissue screening for DEGs. Volcano plot: DEGs following (A) MCAO/R injury vs Sham group and (B) following FGF21 treatment vs MCAO/R group. Heatmap: Top 50 DEGs following (C) MCAO/R injury vs Sham group and (D) following FGF21 treatment vs MCAO/R group.

down-regulated genes were mainly concentrated signal transduction, metabolism, immune system, metabolism of proteins, post-translational protein modification, and gene expression (transcription), among others (Figure 6F). Collectively, FGF21 can be pivotal in the CIRI pathological process via various molecular and signaling mechanisms.

CYBB Potentially Emerges as a Pivotal Effector Molecule of FGF21, Is Crucial in Mediating the Inhibition of Ferroptosis

Here, we intersected the DEGs after IRI and after FGF21 treatment with the 484 ferroptosis-correlated genes reported in the FerrDb database (<http://www.zhounan.org/ferrdb/>) using a Venn diagram, revealing 25 ferroptosis-related DEGs (Figure 7A). The significant difference rate was 5.17%, higher than the 3.62% significant difference rate for other genes (Figure 7B), suggesting that FGF21 has a crucial regulatory function in ferroptosis. The top four ferroptosis-related genes with significant differential expression were analyzed both after IRI and after FGF21 treatment. The results showed that CYBB had the highest fold change in differential expression (Figure 7C). The qPCR findings validated that the expression difference of CYBB mRNA was also the most significant, significantly overexpressed after IRI and repressed after FGF21 treatment (Figure 7D). Western blot results also

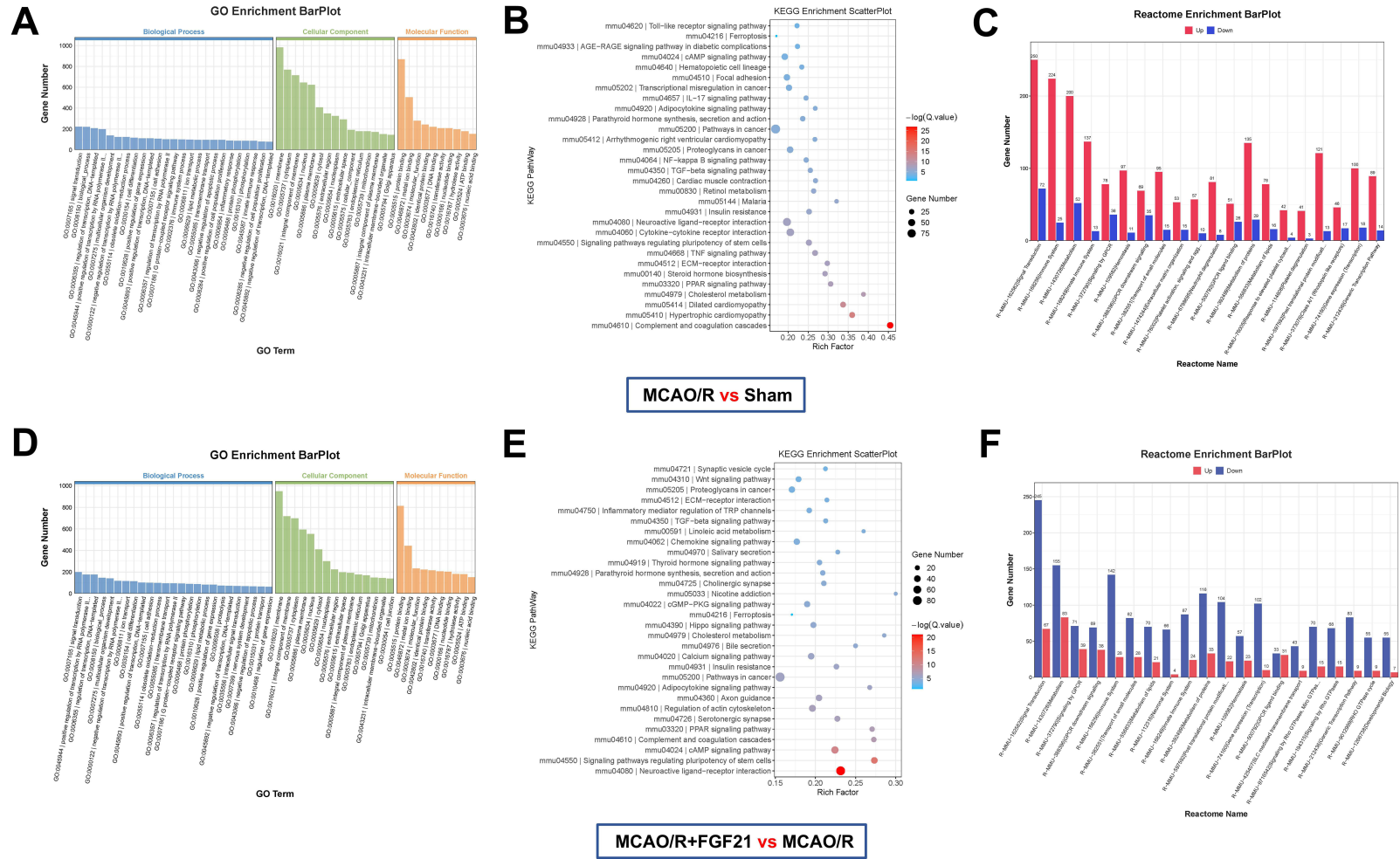


Figure 6 GO, KEGG, and Reactome enrichment analyses of DEGs. Compared to Sham group: **(A)** Bar charts: GO analysis of DEGs after MCAO/R injury; **(B)** Bubble plot: KEGG analysis, highlighting the top 30 significantly enriched pathways after MCAO/R injury; **(C)** Bar charts: Reactome analysis after MCAO/R injury. Compared to the MCAO/R group: **(D)** Bar charts: GO analysis of DEGs after FGF21 treatment; **(E)** Bubble plot: KEGG analysis, emphasizing the top 30 significantly enriched pathways after FGF21 treatment; **(F)** Bar charts: Reactome analysis after FGF21 treatment.

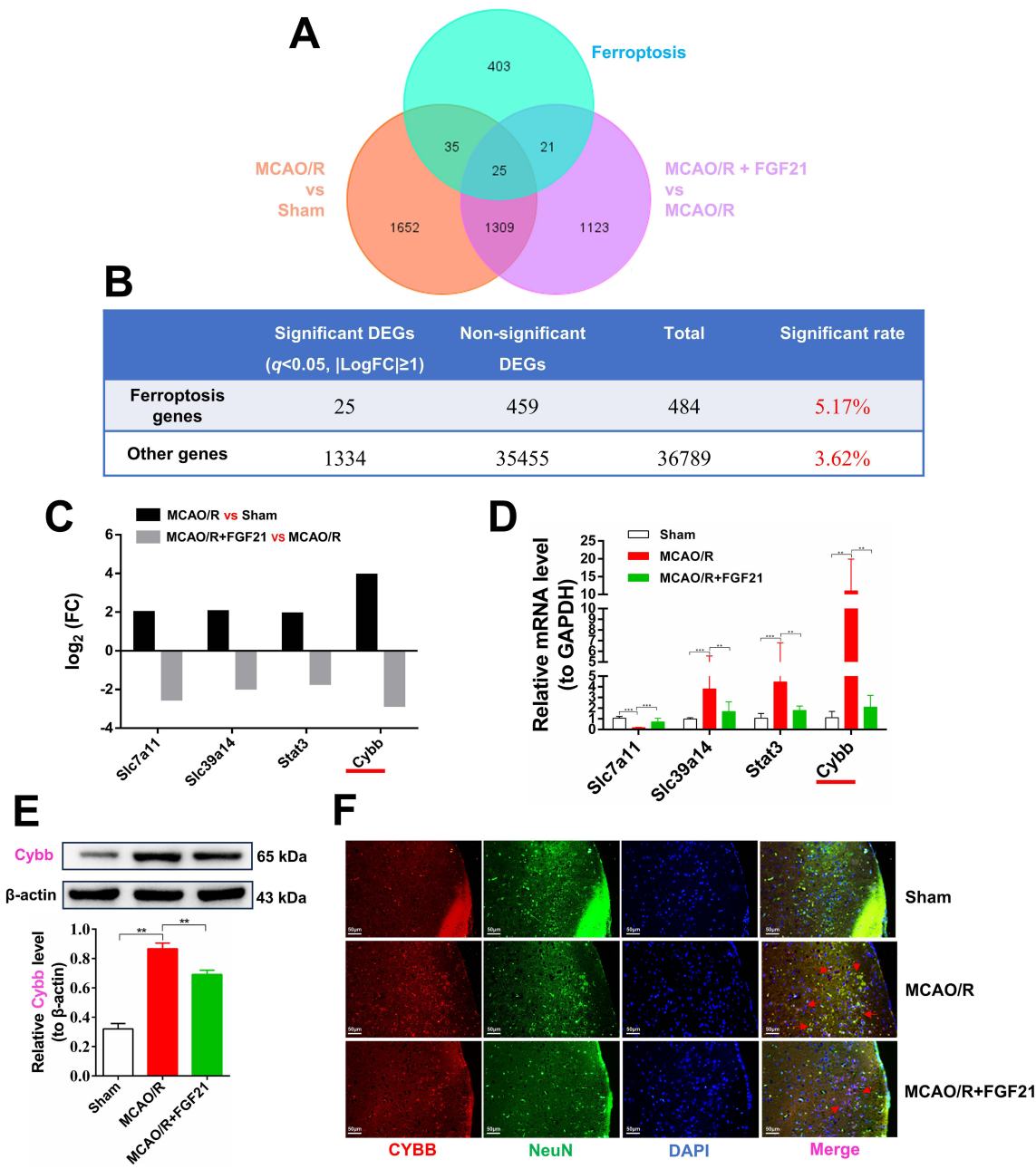


Figure 7 CYBB may be a key effector of FGF21, crucial for inhibiting ferroptosis. **(A)** Venn diagram: Overlap between DEGs and ferroptosis-related genes. **(B)** Comparison of significant differential expression rates for ferroptosis-related vs other genes. **(C)** RNA sequencing: Expression fold changes for the top four significantly altered ferroptosis-related genes. **(D)** qPCR: Relative expression levels for the top four ferroptosis-related genes with significant fold changes. **(E)** Western blotting: CYBB protein expression levels. **(F)** Immunofluorescence double-labeling staining: CYBB and the neuronal-specific marker NeuN. Data represent Mean \pm SD; ($n = 5$). $**P < 0.01$, $***P < 0.001$. The red arrows: Double-labeled immunofluorescent positive cells.

validated that CYBB protein expression in the ischemic penumbra tissue was significantly overexpressed after IRI and suppressed after FGF21 treatment (Figure 7E). Additionally, double immunofluorescence staining with the neuronal-specific markers NeuN and CYBB revealed that CYBB is expressed in cortical neurons, with a significant overexpression after IRI and a significant decrease after FGF21 treatment (Figure 7F). Taken together, CYBB is pivotal in inhibiting ferroptosis by FGF21 after IRI.

Discussion

The FGF21, a potent fibroblast growth factor endowed with a diverse array of biological effects, is indispensable in governing energy homeostasis along with glucose and lipid metabolism.^{28–30} Additionally, FGF21 stands as a pivotal metabolic regulator

while also demonstrating a vital therapeutic role in treating numerous conditions, including alcoholism,³¹ severe hyperlipidemia,³² and intracranial hemorrhage,³³ among others. Limited research has been conducted on the role of FGF21 in CIRI, and its underlying mechanism remains to be elucidated. Previous research has revealed that the administration of 1.5 mg/kg of FGF21 via intraperitoneal injection significantly reduces the infarct volume in rats subjected to CIRI after 24 h.³⁴ Furthermore, additional studies have demonstrated that this dosage of FGF21 not only diminishes the infarct volume in mice experiencing IRI but also attenuates the neuroinflammatory response post-reperfusion by modulating the spatiotemporal dynamics of microglia/macrophages.³⁵ Consistently, the findings of our current study underscore that treatment with 1.5 mg/kg of FGF21 significantly decreases the infarct volume in mice. Moreover, our results further reveal a significantly diminished number of apoptotic neurons at the ischemic site following FGF21 treatment, accompanied by a significant alleviation of pathological damage in the ischemic brain tissue. These observations underscore the therapeutic efficacy of FGF21 in mitigating CIRI.

The pathological processes such as OxS, inflammation, and neuronal apoptosis following CIR inflict varying degrees of damage to the ischemic brain tissue, exacerbating patients' prognosis.³⁶ The OxS, triggered post-I/R, results in the massive generation of ROS, intensifying lipid peroxidation. The accumulation of intracellular Fe^{2+} further propels cells towards ferroptosis, a form of cell death. Numerous studies have underscored the pivotal role of ferroptosis in CIRI. Moreover, excessive iron accumulation in this context exacerbates OxS, triggering cellular damage and demise.³⁷ Interventions targeting ferroptosis can significantly ameliorate CIRI. By modulating OxS, iron metabolism, and reducing iron accumulation, the mortality rate of neurons after I/R can be effectively mitigated.³⁸ Existing research has confirmed the beneficial effects of FGF21 in inhibiting OxS, encompassing its ability to ameliorate lung fibrosis by alleviating OxS,³⁹ improve collagen-provoked arthritis by modulating OxS and inhibiting nuclear factor- κB signaling,⁴⁰ and protect mouse livers from d-galactose-triggered OxS and apoptosis by activating the Nrf2 and PI3K/Akt pathways. The findings of this study demonstrate significantly reduced pro-oxidant ROSs, MDA, and MPA concentrations in the serum of FGF21-treated mice, coupled with increased antioxidant SOD concentration. Furthermore, the concentration of ROS in the ischemic penumbra brain tissue was also significantly decreased, suggesting that FGF21 exerts an inhibitory effect on OxS during the treatment of CIRI. This observation aligns with recent reports on the antioxidant stress role of FGF21 in other diseases. Currently, scholars have reported the inhibitory impact of FGF21 on ferroptosis in various diseases. Ye et al have demonstrated that FGF21 alleviated lung IRI by inhibiting endoplasmic reticulum stress-provoked ferroptosis by activating FGFR1/PPAR δ signaling.⁴¹ Zhang et al have found that FGF21 mitigated calcium oxalate-triggered oxidative damage and ferroptosis in renal tubular epithelium by activating Nrf2 signaling.⁴² Furthermore, Yan et al have confirmed that FGF21 promotes the repair of damaged peripheral nerves by inhibiting ferroptosis arising from mitochondrial dysfunction.⁴³ Our research uncovered that in mice treated with FGF21, there was a significant decrease in the concentrations of Fe^{2+} and oxidized glutathione (GSSG) within the ischemic penumbra of the brain tissue, coupled with a significant increase in the concentration of reduced glutathione (GSH). Additionally, the ferroptosis-promoting protein ACSL4 was significantly down-regulated, while the ferroptosis-suppressing protein GPX4 was overexpressed. Hence, our findings suggest that FGF21 may further exert its anti-ferroptotic effects by combating OxS. Importantly, this study also provides the first experimental evidence that FGF21 exhibits neuroprotective effects against ferroptosis in diseases such as CIRI.

For further elucidation of the molecular mechanisms behind the implication of FGF21 in CIRI, we conducted comprehensive transcriptomic sequencing of ischemic penumbra brain tissues. Our findings revealed significant differential expression of numerous genes before and after FGF21 treatment, encompassing pivotal molecules associated with inflammatory responses and OxS, such as Stat3, Tlr9, and Cybb, as well as diverse transcription factors (including Klf12 and Aff2) and ubiquitination enzymes (such as Rnf152). These results indicate that FGF21 exerts pleiotropic effects in CIRI through intricate molecular regulatory mechanisms. Moreover, GO, KEGG and Reactome enrichment analyses of the DEGs demonstrated their widespread involvement in biological processes subsequent to CIR, encompassing signal transduction, metabolic regulation, ion transport, DNA and protein binding, and the modulation of signaling pathways related to inflammation, OxS, and ferroptosis. These findings further underscore the multifaceted regulatory roles of FGF21 in the pathological processes of CIRI, with the specific mechanisms awaiting further experimental validation.

This study revealed that FGF21 not only ameliorates pathological damage in ischemic brain tissues but also inhibits OxS and ferroptosis. Further analysis indicated a significantly higher rate of significant differences in genes associated with ferroptosis compared to other genes, emphasizing the pivotal role of FGF21 in modulating ferroptosis processes following CIRI. Among the significantly altered ferroptosis-related genes, we observed the most significant difference in the expression of cytochrome b-245,

beta polypeptide (CYBB) gene before and after FGF21 treatment. Subsequent experimental validation demonstrated that the CYBB protein is expressed in neurons, with a marked up-regulation post-reperfusion injury and a significant down-regulation following FGF21 therapy. The CYBB, termed NOX₂, is composed of cytochrome b-245, a vital protein of the phagocytic NADPH oxidase. Upon activation, it generates a surge of bactericidal superoxide and other oxides, resulting in a rapid ROS accumulation.⁴⁴ Recently, research has suggested that CYBB may serve as a crucial molecule promoting ferroptosis, as its up-regulated expression leads to massive production and accumulation of lipid ROS, further inducing lipid peroxidation and Fe²⁺ deposition, ultimately triggering ferroptosis in various disease cells, including those involved in Huntington's disease and abdominal aortic aneurysm.^{45,46} Furthermore, CYBB may facilitate ferroptosis through various downstream mechanisms. Xu et al⁴⁷ have demonstrated that NOX₂ triggers ferroptosis by inhibiting the STAT3/GPX4 pathway, thereby exacerbating preeclampsia. Additionally, Song et al⁴⁸ have revealed that the activation of NOX₂ mediates the ferroptosis-promoting effect of HAND2-AS1 by enhancing the expression of DUOX₂. Accordingly, we speculate that inhibiting neuronal ferroptosis by FGF21 after ischemia-reperfusion may be associated with its negative regulation of CYBB. However, the underlying mechanisms await further experimental validation.

This study reveals that FGF21 can reduce the cerebral infarction volume and ameliorate pathological damage in the brain tissue of mice subjected to ischemic reperfusion injury while also inhibiting OxS and ferroptosis. Furthermore, our findings imply that CYBB may be a pivotal gene in regulating neuronal ferroptosis following FGF21 reperfusion injury. Compared with previous research, our study demonstrates that FGF21 exhibits both antioxidant stress effects similar to Puerarin⁴⁹ and ferroptosis inhibition akin to Baicalein⁵⁰ in CIRI treatment in mice, confirming the therapeutic efficacy of FGF21. Nonetheless, further research should compare the therapeutic efficacy of different drugs. Additionally, the potential side effects of FGF21 remain unclear, and the significance of its long-term treatment, as well as its ability to improve long-term neurological prognosis, warrants further investigation. Although significant challenges remain in the clinical translation of FGF21, including considerations of toxicity, side effects, and safety, it is encouraging that Phase II clinical trials of FGF21 formulations for treating Type 2 diabetes in obese patients have shown promising efficacy with low side effects,⁵¹ offering hope for using FGF21 in treating clinical stroke patients. Our study also has some drawbacks: first, the role of FGF21 in OxS and ferroptosis following CIRI lacks validation through in vitro cellular experiments. Additionally, functional validation of the role of CYBB is lacking. Therefore, we will continue our in-depth in vitro and in vivo experimental research on the function of CYBB in CIRI and the mechanism by which FGF21 regulates CYBB to exert anti-ferroptotic effects.

Conclusion

Our study, for the first time, reports that FGF21 protects CIRI by inhibiting OxS and ferroptosis; CYBB, a new key regulator, may mediate its anti-ferroptotic effects (Figure 8). This discovery offers new insights into therapies for CIRI.

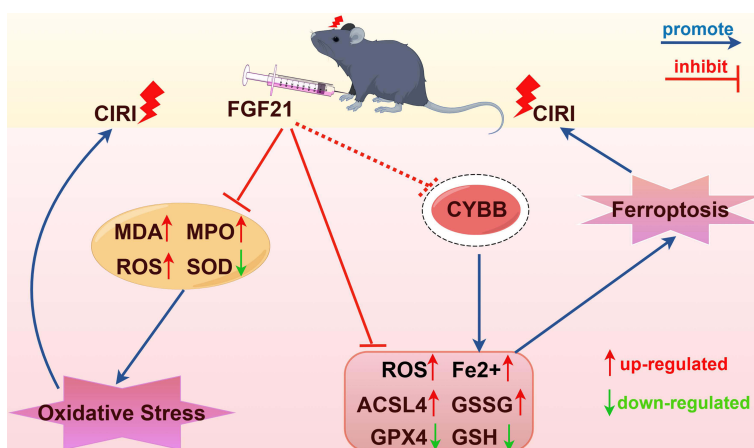


Figure 8 Schematic representation of the mechanisms by which FGF21 influences CIRI. FGF21 protects CIRI by inhibiting OxS and ferroptosis; CYBB, a new key regulator, may mediate its anti-ferroptotic effects.

Abbreviations

FGF21, fibroblast growth factor 21; CIRI, cerebral ischemia/reperfusion injury; IRI, ischemia/reperfusion injury; MCAO/R, middle cerebral artery occlusion / reperfusion; OxS, oxidative stress; CYBB, cytochrome b-245, beta polypeptide; ROS, reactive oxygen species; MDA, malondialdehyde; MPO, myeloperoxidase; SOD, superoxide dismutase; DEGs, differentially expressed genes.

Data Sharing Statement

The datasets for this study are available from the corresponding author upon request.

Funding

This work was funded by the Joint Key Project of Applied Basic Research of Yunnan Province (Grant No.202201AY070001–037), and the Joint General Project of Applied Basic Research of Yunnan Province (Grant No. 202101AY070001–116), and the “535” High-Level Talent Young Backbone Training Program of the First Affiliated Hospital of Kunming Medical University (Grant No. 2024535Q13).

Disclosure

The authors report no conflicts of interest in this work.

References

1. Feigin VL, Stark BA, Johnson CO. GBD 2019 Stroke Collaborators. Global, regional, and national burden of stroke and its risk factors, 1990–2019: a systematic analysis for the Global Burden of Disease Study 2019. *Lancet Neurol.* **2021**;20(10):795–820. doi:10.1016/S1474-4422(21)00252-0
2. Zhang T, Wang Y, Xia Q, et al. Propofol Mediated Protection of the Brain From Ischemia/Reperfusion Injury Through the Regulation of Microglial Connexin 43. *Front Cell Dev Biol.* **2021**;9:637233. doi:10.3389/fcell.2021.637233
3. Li M, Tang H, Li Z, et al. Emerging Treatment Strategies for Cerebral Ischemia-Reperfusion Injury. *Neuroscience.* **2022**;507:112–124. doi:10.1016/j.neuroscience.2022.10.020
4. Zheng T, Jiang T, Huang Z, et al. Role of traditional Chinese medicine monomers in cerebral ischemia/reperfusion injury: a review of the mechanism. *Front Pharmacol.* **2023**;14:1220862. doi:10.3389/fphar.2023.1220862
5. Wang W, Lu D, Shi Y, et al. Exploring the Neuroprotective Effects of Lithium in Ischemic Stroke: a literature review. *Int J Med Sci.* **2024**;21(2):284–298. doi:10.7150/ijms.88195
6. Liu X, Xie C, Wang Y, et al. Ferritinophagy and Ferroptosis in Cerebral Ischemia Reperfusion Injury. *Neurochem Res.* **2024**;49(8):1965–1979. doi:10.1007/s11064-024-04161-5
7. Xu P, Kong L, Tao C, et al. Elabela-APJ axis attenuates cerebral ischemia/reperfusion injury by inhibiting neuronal ferroptosis. *Free Radic Biol Med.* **2023**;196:171–186. doi:10.1016/j.freeradbiomed.2023.01.008
8. Delgado-Martín S, Martínez-Ruiz A. The role of ferroptosis as a regulator of oxidative stress in the pathogenesis of ischemic stroke. *FEBS Lett.* **2024**;598(17):2160–2173. doi:10.1002/1873-3468.14894
9. Liu D, Yang S, Yu S. Interactions Between Ferroptosis and Oxidative Stress in Ischemic Stroke. *Antioxidants.* **2024**;13(11):1329. doi:10.3390/antiox13111329
10. Ren J, Li C, Yan X, et al. Crosstalk between Oxidative Stress and Ferroptosis/Oxytosis in Ischemic Stroke: possible Targets and Molecular Mechanisms. *Oxid Med Cell Longev.* **2021**;2021(1):6643382. doi:10.1155/2021/6643382
11. Fisher FM, Maratos-Flier E. Understanding the Physiology of FGF21. *Annu Rev Physiol.* **2016**;78(1):223–241. doi:10.1146/annurev-physiol-021115-105339
12. Tezze C, Romanello V, Sandri M. FGF21 as Modulator of Metabolism in Health and Disease. *Front Physiol.* **2019**;10:419. doi:10.3389/fphys.2019.00419
13. Kharitonov A, Shyanova TL, Koester A, et al. FGF-21 as a novel metabolic regulator. *J Clin Invest.* **2005**;115(6):1627–1635. doi:10.1172/JCI23606
14. Geng L, Lam KSL, Xu A. The therapeutic potential of FGF21 in metabolic diseases: from bench to clinic. *Nat Rev Endocrinol.* **2020**;16(11):654–667. doi:10.1038/s41574-020-0386-0
15. Salminen A, Kaamiranta K, Kauppinen A. Regulation of longevity by FGF21: interaction between energy metabolism and stress responses. *Ageing Res Rev.* **2017**;37:79–93. doi:10.1016/j.arr.2017.05.004
16. Hsueh H, Pan W, Kastin AJ. The fasting polypeptide FGF21 can enter brain from blood. *Peptides.* **2007**;28(12):2382–2386. doi:10.1016/j.peptides.2007.10.007
17. Tan BK, Hallschmid M, Adya R, et al. Fibroblast growth factor 21 (FGF21) in human cerebrospinal fluid: relationship with plasma FGF21 and body adiposity. *Diabetes.* **2011**;60(11):2758–2762. doi:10.2337/db11-0672
18. Wang Q, Yuan J, Yu Z, et al. FGF21 Attenuates High-Fat Diet-Induced Cognitive Impairment via Metabolic Regulation and Anti-inflammation of Obese Mice. *mol Neurobiol.* **2018**;55(6):4702–4717. doi:10.1007/s12035-017-0663-7
19. Kang K, Xu P, Wang M, et al. FGF21 attenuates neurodegeneration through modulating neuroinflammation and oxidant-stress. *Biomed Pharmacother.* **2020**;129:110439. doi:10.1016/j.biopha.2020.110439

20. Chen J, Hu J, Liu H, et al. FGF21 Protects the Blood-Brain Barrier by Upregulating PPAR γ via FGFR1/ β -klotho after Traumatic Brain Injury. *J Neurotrauma*. 2018;35(17):2091–2103. doi:10.1089/neu.2017.5271
21. Wu A, Feng B, Yu J, et al. Fibroblast growth factor 21 attenuates iron overload-induced liver injury and fibrosis by inhibiting ferroptosis. *Redox Biol*. 2021;46:102131. doi:10.1016/j.redox.2021.102131
22. Xu T, Zhu Q, Huang Q, et al. FGF21 prevents neuronal cell ferroptosis after spinal cord injury by activating the FGFR1/ β -Klotho pathway. *Brain Res Bull*. 2023;202:110753. doi:10.1016/j.brainresbull.2023.110753
23. Bai W, Huo S, Zhou G, et al. Biliverdin modulates the Nrf2/A20/EF1A2 axis to alleviate cerebral ischemia-reperfusion injury by inhibiting pyroptosis. *Biomed Pharmacother*. 2023;165:115057. doi:10.1016/j.biopha.2023.115057
24. Meng Y, Ding Z, Wang H, et al. Effect of microRNA-155 on angiogenesis after cerebral infarction of rats through AT1R/VEGFR2 pathway. *Asian Pac J Trop Med*. 2015;8(10):829–835. doi:10.1016/j.apjtm.2015.09.009
25. Arifin WN, Zahiruddin WM. Sample Size Calculation in Animal Studies Using Resource Equation Approach. *Malays J Med Sci*. 2017;24(5):101–105. doi:10.21315/mjms2017.24.5.11
26. Ding P, Yang R, Li C, et al. Fibroblast growth factor 21 attenuates ventilator-induced lung injury by inhibiting the NLRP3/caspase-1/GSDMD pyroptotic pathway. *Crit Care*. 2023;27(1):196. doi:10.1186/s13054-023-04488-5
27. Hu Q, Chen C, Yan J, et al. Therapeutic application of gene silencing MMP-9 in a middle cerebral artery occlusion-induced focal ischemia rat model. *Exp Neurol*. 2009;216(1):35–46. doi:10.1016/j.expneurol.2008.11.007
28. Recinella L, Leone S, Ferrante C, et al. Effects of central fibroblast growth factor 21 (FGF21) in energy balance. *J Biol Regul Homeost Agents*. 2017;31(3):603–613.
29. Cuevas-Ramos D, Aguilar-Salinas CA, Gómez-Pérez FJ. Metabolic actions of fibroblast growth factor 21. *Curr Opin Pediatr*. 2012;24(4):523–529. doi:10.1097/MOP.0b013e3283557d22
30. Huang Z, Xu A, Cheung BMY. The Potential Role of Fibroblast Growth Factor 21 in Lipid Metabolism and Hypertension. *Curr Hypertens Rep*. 2017;19(4):28. doi:10.1007/s11906-017-0730-5
31. Flippo KH, Trammell SAJ, Gillum MP, et al. FGF21 suppresses alcohol consumption through an amygdalo-striatal circuit. *Cell Metab*. 2022;34(2):317–328.e316. doi:10.1016/j.cmet.2021.12.024
32. Bhatt DL, Bays HE, Miller M, et al. The FGF21 analog pegozafermin in severe hypertriglyceridemia: a randomized Phase 2 trial. *Nat Med*. 2023;29(7):1782–1792. doi:10.1038/s41591-023-02427-z
33. Wang R, Wang J, Zhang Z, et al. FGF21 alleviates endothelial mitochondrial damage and prevents BBB from disruption after intracranial hemorrhage through a mechanism involving SIRT6. *Mol Med*. 2023;29(1):165. doi:10.1186/s10020-023-00755-x
34. Yang X, Hui Q, Yu B, et al. Design and Evaluation of Lyophilized Fibroblast Growth Factor 21 and Its Protection against Ischemia Cerebral Injury. *Bioconjug Chem*. 2018;29(2):287–295. doi:10.1021/acs.bioconjchem.7b00588
35. Wang D, Liu F, Zhu L, et al. FGF21 alleviates neuroinflammation following ischemic stroke by modulating the temporal and spatial dynamics of microglia/macrophages. *J Neuroinflammation*. 2020;17(1):257. doi:10.1186/s12974-020-01921-2
36. El Khashab IH, Abdelsalam RM, Elbrairy AI, et al. Chrysin attenuates global cerebral ischemic reperfusion injury via suppression of oxidative stress, inflammation and apoptosis. *Biomed Pharmacother*. 2019;112:108619. doi:10.1016/j.biopha.2019.108619
37. Shen L, Gan Q, Yang Y, et al. Mitophagy in Cerebral Ischemia and Ischemia/Reperfusion Injury. *Front Aging Neurosci*. 2021;13:687246. doi:10.3389/fnagi.2021.687246
38. Bayraktar A, Erbaş D, Akarca Dizakar S, et al. The Effect of Hepcidin on Cardiac Ischemia-Reperfusion Injury. *J Invest Surg*. 2020;33(9):813–821. doi:10.1080/08941939.2019.1579275
39. Zhang S, Yu D, Wang M, et al. FGF21 attenuates pulmonary fibrogenesis through ameliorating oxidative stress in vivo and in vitro. *Biomed Pharmacother*. 2018;103:1516–1525. doi:10.1016/j.biopha.2018.03.100
40. Yu Y, Li S, Liu Y, et al. Fibroblast growth factor 21 (FGF21) ameliorates collagen-induced arthritis through modulating oxidative stress and suppressing nuclear factor-kappa B pathway. *Int Immunopharmacol*. 2015;25(1):74–82. doi:10.1016/j.intimp.2015.01.005
41. Ye X, Pei F, Li W, et al. Fibroblast growth factor 21 attenuates pulmonary ischemia/reperfusion injury via inhibiting endoplasmic reticulum stress-induced ferroptosis through FGFR1/PPAR δ signaling pathway. *Int Immunopharmacol*. 2024;143:113307. doi:10.1016/j.intimp.2024.113307
42. Zhang J, Zhang G, Jiang L, et al. FGF21 relieves calcium oxalate-induced cell injury, apoptosis, oxidative damage and ferroptosis of renal tubular epithelial cells through activating Nrf2 signaling pathway. *Cytotechnology*. 2024;76(5):519–531. doi:10.1007/s10616-024-00633-2
43. Yan Y, Ran X, Zhou Z, et al. FGF21 inhibits ferroptosis caused by mitochondrial damage to promote the repair of peripheral nerve injury. *Front Pharmacol*. 2024;15:1358646. doi:10.3389/fphar.2024.1358646
44. Wang Z, Liu T, Wang Z, et al. CYBB-Mediated Ferroptosis Associated with Immunosuppression in Mycobacterium leprae-Infected Monocyte-Derived Macrophages. *J Invest Dermatol*. 2024;144(4):874–887.e872. doi:10.1016/j.jid.2023.10.012
45. Okada N, Nakamura S, Shimazawa M. 3-Nitropropionic Acid Enhances Ferroptotic Cell Death via NOX2-Mediated ROS Generation in STHDhQ111 Striatal Cells Carrying Mutant Huntingtin. *Biol Pharm Bull*. 2023;46(2):177–186. doi:10.1248/bpb.b22-00529
46. Filiberto AC, Ladd Z, Leroy V, et al. Resolution of inflammation via RvD1/FPR2 signaling mitigates Nox2 activation and ferroptosis of macrophages in experimental abdominal aortic aneurysms. *FASEB J*. 2022;36:e22579. doi:10.1096/fj.202201114R.
47. Xu X, Zhu M, Zu Y, et al. Nox2 inhibition reduces trophoblast ferroptosis in preeclampsia via the STAT3/GPX4 pathway. *Life Sci*. 2024;343:122555. doi:10.1016/j.lfs.2024.122555
48. Song Z, Zhang Y, Luo W, et al. HAND2-AS1 Promotes Ferroptosis to Reverse Lenvatinib Resistance in Hepatocellular Carcinoma by TLR4/NOX2/DUOX2 Axis. *Curr Cancer Drug Targets*. 2024;25:144–158.
49. Zhang Q, Yao M, Qi J, et al. Puerarin inhibited oxidative stress and alleviated cerebral ischemia-reperfusion injury through PI3K/Akt/Nrf2 signaling pathway. *Front Pharmacol*. 2023;14:1134380. doi:10.3389/fphar.2023.1134380
50. Li M, Meng Z, Yu S, et al. Baicalein ameliorates cerebral ischemia-reperfusion injury by inhibiting ferroptosis via regulating GPX4/ACSL4/ACSL3 axis. *Chem Biol Interact*. 2022;366:110137. doi:10.1016/j.cbi.2022.110137
51. Charles ED, Neuschwander-Tetri BA, Pablo Frias J, et al. Pegbelfermin (BMS-986036), PEGylated FGF21, in Patients with Obesity and Type 2 Diabetes: results from a Randomized Phase 2 Study. *Obesity*. 2019;27(1):41–49. doi:10.1002/oby.22344

Neuropsychiatric Disease and Treatment**Dovepress**
Taylor & Francis Group**Publish your work in this journal**

Neuropsychiatric Disease and Treatment is an international, peer-reviewed journal of clinical therapeutics and pharmacology focusing on concise rapid reporting of clinical or pre-clinical studies on a range of neuropsychiatric and neurological disorders. This journal is indexed on PubMed Central, the 'PsycINFO' database and CAS, and is the official journal of The International Neuropsychiatric Association (INA). The manuscript management system is completely online and includes a very quick and fair peer-review system, which is all easy to use. Visit <http://www.dovepress.com/testimonials.php> to read real quotes from published authors.

Submit your manuscript here: <https://www.dovepress.com/neuropsychiatric-disease-and-treatment-journal>